We are IntechOpen,
the world's leading publisher of
Open Access books
Built by scientists, for scientists

6,900
Open access books available

186,000
International authors and editors

200M
Downloads

Our authors are among the

154
Countries delivered to

TOP 1%
most cited scientists

12.2%
Contributors from top 500 universities

BOOK CITATION INDEX
CLARIVATE ANALYTICS
INDEXED

WEB OF SCIENCE™

Selection of our books indexed in the Book Citation Index
in Web of Science™ Core Collection (BKCI)

Interested in publishing with us?
Contact book.department@intechopen.com

Numbers displayed above are based on latest data collected.
For more information visit www.intechopen.com

1

F-Transform Based Image Fusion

I. Perfilieva, M. Daňková, P. Hoďáková and M. Vajgl
Institute for Research and Applications of Fuzzy Modeling, University of Ostrava
Czech Republic

1. Introduction

Developments in hardware, sensor quality and imaging technology have attracted a great deal of research interest in image processing and associated fields in the last two decades. Here, we focus particularly on the problem of image fusion due to the fact that it is one of the leading areas of intense research and development activity. Moreover, image fusion is used in many real-world applications such as medical diagnosis with multimodal images (for an overview of medical applications, see Constantinos et al. (2001)), person or weapon detection by automated defense systems and classification of objects (e.g., roads, rivers, mountains and towns) in multi-sensor geographical images. (a wide overview of applications can be found in Piella (2003)).

Image fusion aims at the integration of various complementary image data into a single, new image with the best possible quality. The term "quality" depends on the demands of the specific application, which is usually related to its usefulness for human visual perception, computer vision or further processing. As stated in Šroubek & Flusser (2005), if u is an ideal image (considered as a function of two variables) and $c_1,\ldots,c_K$ are acquired images, then the relation between each c_i and u can be expressed by

$$c_i(x,y) = d_i(u(x,y)) + e_i(x,y),\ i = 1,\ldots,K$$

where d_i is an unknown operator describing the image degradation, and e_i is an additive random noise.

Image fusion is a means to obtain an image $\hat{u}$ that yields in some sense a better representation of the ideal image u than is provided by each individual image c_i. There are various fusion methodologies currently in use. The main categories are determined by the level at which the fusion is actually executed Zhang (2010). The methodologies are designed on the basis of the following mathematical fields: statistical methods (e.g., using aggregation operators, such as the MinMax method Blum (2005)), estimation theory Loza et al. (2010), fuzzy methods (see Singh et al. (2004); Ranjan et al. (2005); Ashoori et al. (2008)), optimization methods (e.g., neural networks, genetic algorithms Mumtaz & Majid (2008)) and multiscale decomposition methods, which incorporate various transforms, e.g., discrete wavelet transforms (for a classification of these methods see Piella (2003); a classification of wavelet-based image fusion methods can be found in Amolins et al. (2007), and for applications for blurred and unregistered images, refer to Šroubek & Flusser (2005); Šroubek & Zítová (2006)). The choice of a fusion methodology is basically influenced by parameters relating to the type of degradation operators d_i, the occurrence of noise and the type of outputs of the preprocessing analysis.

The main purpose of this contribution is to show that the F-transform technique is a promising and efficient method for image fusion Daňková & Valášek (2006); Perfilieva & Daňková (2008). The original motivation for the F-transform (an abbreviated name for the fuzzy transform) came from fuzzy modeling Perfilieva (2006; 2007). The purpose was to show that, similarly to traditional transforms (Fourier and wavelet), the F-transform performs a transformation of an original universe of functions into a universe of their "skeleton models" (vectors of F-transform components) in which further computation is easier (e.g., an application to the initial-value problem with a fuzzy initial condition Perfilieva, De Meyer, De Baets & Plšková (2008)). In this respect, the F-transform can be as useful in many applications as traditional transforms (see applications to image compression Perfilieva, Pavliska, Vajgl & De Baets (2008) and time-series procession Perfilieva, Novák, Pavliska, Dvořák & Štěpnička (2008)). Moreover, sometimes the F-transform can be more efficient than its counterparts. Without going into specific details here, we claim that F-transform has a potential advantage over the wavelet transform; while the latter uses a single "mother wavelet" that determines all basic functions, the former can use basic functions with different shapes.

This contribution is organized as follows: Section 2 introduces the F-transform technique and gives an overview of its properties; Section 3 describes the details of image representation for image fusion using the F-transform; Section 4 provides the details of two algorithms (where the first algorithm is a special case of the second one) for image fusion that use image representation based on the F-transform; Section 5 addresses some particular problems in image fusion and highlights the advantages of the optional setting in the introduced algorithm. Finally, conclusions, comments and some future trends in our research are given in the Section 6.

2. F-transform

To find a fused image, we propose two algorithms that are based on the F-transform technique. Before going into the details of image fusion, we give a general characterization and the relevant details of the technique developed herein.

Generally speaking, the F-transform produces an image by a linear mapping from a set of ordinary continuous/discrete functions over a domain P onto a set of functions within a fuzzy partition of P. We assume that the reader is familiar with the notion of the *fuzzy set* and how is it represented.

Below, we explain the F-transform in more detail and adapt our explanation to the purpose of this chapter (we refer to Perfilieva (2006) for a complete description). The explanation will be given for the example of a discrete function that corresponds to the image u.

Let u be represented by the discrete function $u : P \to \mathbb{R}$ of two Variables, where $P = \{(i,j) \mid i = 1,\ldots,N, j = 1,\ldots,M\}$ is an $N \times M$ array of pixels, and $\mathbb{R}$ is the set of reals. If $(i,j) \in P$ is a pixel, then $u(i,j)$ represents its intensity range.

The F-transform of u corresponds u to the matrix $\mathbf{F}_{nm}[u]$ of F-transform components:

$$\mathbf{F}_{nm}[u] = \begin{pmatrix} F[u]_{11} & \ldots & F[u]_{1m} \\ \vdots & \vdots & \vdots \\ F[u]_{n1} & \ldots & F[u]_{nm} \end{pmatrix}. \tag{1}$$

Each component $F[u]_{kl}$ is a local mean value of u over a support set of the respective fuzzy set $A_k \times B_l$. The latter is an element of a *fuzzy partition* of the Cartesian product of intervals

$[1, N] \times [1, M]$. Using the fact that a fuzzy partition of a Cartesian product is the Cartesian product of fuzzy partitions, we first introduce this notion for a single interval and then for a Cartesian product of intervals.

Let $[1, N] = \{x \mid 1 \le x \le N\}$ be an interval on the real line $\mathbb{R}$, $n \ge 2$, a number of fuzzy sets in a fuzzy partition of $[1, N]$, and $h = \frac{N-1}{n-1}$ the distance between nodes $x_1, \ldots, x_n \in [1, N]$, where $x_1 = 1$, $x_k = x_1 + (k-1)h$, $k = 1, \ldots, n$. Fuzzy sets $A_1, \ldots, A_n : [1, N] \to [0, 1]$ establish a *h-uniform fuzzy partition* of $[1, N]$ if the following requirements are fulfilled:

   (i) for every $k = 1, \ldots, n$, $A_k(x) = 0$ if $x \in [1, N] \setminus [x_{k-1}, x_{k+1}]$, where $x_0 = x_1$, $x_{N+1} = x_N$;

  (ii) for every $k = 1, \ldots, n$, A_k is continuous on $[x_{k-1}, x_{k+1}]$, where $x_0 = x_1$, $x_{N+1} = x_N$;

 (iii) for every $i = 1, \ldots, N$, $\sum_{k=1}^{n} A_k(i) = 1$;

  (iv) for every $k = 1, \ldots, n$, $\sum_{i=1}^{N} A_k(i) > 0$;

   (v) for every $k = 2, \ldots, n-1$, A_k is symmetrical with respect to the line $x = x_k$.

The membership functions of the respective fuzzy sets in a fuzzy partition are called *basic functions*. The example of triangular basic functions $A_1, \ldots, A_n$, $n \ge 2$ on the interval $[1, N]$ is given below.

$$A_1(x) = \begin{cases} 1 - \frac{(x - x_1)}{h}, & x \in [x_1, x_2], \\ 0, & \text{otherwise}, \end{cases}$$

$$A_k(x) = \begin{cases} \frac{|x - x_k|}{h}, & x \in [x_{k-1}, x_{k+1}], \\ 0, & \text{otherwise}, \end{cases}$$

$$A_n(x) = \begin{cases} \frac{(x - x_{n-1})}{h}, & x \in [x_{n-1}, x_n], \\ 0, & \text{otherwise}. \end{cases}$$

Note that the shape (e.g., triangular or sinusoidal) of a basic function in a fuzzy partition is not predetermined and can be chosen according to additional requirements.

We now introduce two *extreme fuzzy partitions* of $[1, N]$ that will be used in the following.

Largest partition. The largest partition contains only one fuzzy set, $A_1 : [1, N] \to [0, 1]$, such that for all $x \in [1, N]$, $A_1(x) = 1$.

Finest partition. The finest partition is established by N fuzzy sets, $A_1, \ldots, A_N : [1, N] \to [0, 1]$, such that for all $k, l = 1, \ldots, N$, $k \neq l$, $A_k(x_k) = 1$ and $A_k(x_l) = 0$.

If fuzzy sets $A_1, \ldots, A_n$ establish a fuzzy partition of $[1, N]$ and $B_1, \ldots, B_m$ do the same for $[1, M]$, then the Cartesian product $\{A_1, \ldots, A_n\} \times \{B_1, \ldots, B_m\}$ of these fuzzy partitions is the set of all fuzzy sets $A_k \times B_l$, $k = 1, \ldots, n$, $l = 1, \ldots, m$. The membership function $A_k \times B_l : [1, N] \times [1, M] \to [0, 1]$ is equal to the product $A_k \cdot B_l$ of the respective membership functions. Fuzzy sets $A_k \times B_l$, $k = 1, \ldots, n$, $l = 1, \ldots, m$ establish a fuzzy partition of the Cartesian product $[1, N] \times [1, M]$. In Figure 1, an example of a fuzzy partition of $[1, 3] \times [1, 4]$ by triangular membership functions is given.

Let $u : P \to \mathbb{R}$ and fuzzy sets $A_k \times B_l$, $k = 1, \ldots, n$, $l = 1, \ldots, m$, establish a fuzzy partition of $[1, N] \times [1, M]$. The (direct) *F-transform* of u (with respect to the chosen partition) is an image of the mapping $F[u] : \{A_1, \ldots, A_n\} \times \{B_1, \ldots, B_m\} \to \mathbb{R}$ defined by
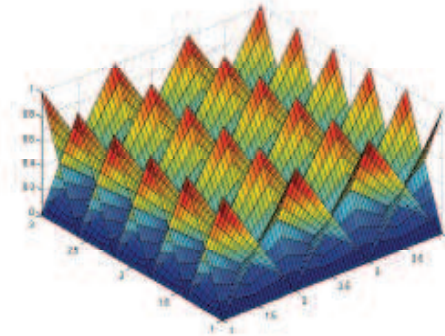
Fig. 1. An example of a fuzzy partition of $[1,3] \times [1,4]$ by triangular membership functions.

$$F[u](A_k \times B_l) = \frac{\sum_{i=1}^{N} \sum_{j=1}^{M} u(i,j) A_k(i) B_l(j)}{\sum_{i=1}^{N} \sum_{j=1}^{M} A_k(i) B_l(j)}, \qquad (2)$$

where $k = 1,\ldots,n, l = 1,\ldots,m$. The value $F[u](A_k \times B_l)$ is called an *F-transform component* of u and is denoted by $F[u]_{kl}$. The components $F[u]_{kl}$ can be arranged into the matrix representation as in (1) or into the vector representation as follows:

$$(F[u]_{11},\ldots,F[u]_{1m},\ldots,F[u]_{n1},\ldots,F[u]_{nm}). \qquad (3)$$

The *inverse F-transform* of u is a function on P, which is represented by the following inversion formula, where $i = 1,\ldots,N, j = 1,\ldots,M$:

$$u_{nm}(i,j) = \sum_{k=1}^{n} \sum_{l=1}^{m} F[u]_{kl} A_k(i) B_l(j). \qquad (4)$$

It can be shown that the inverse F-transform u_{nm} approximates the original function u on the domain P. The proof can be found in Perfilieva (2006; 2007).

Example 1 *Let discrete real function $u = u(x,y)$ be defined on the $N \times M$ array of pixels $P = \{(i,j) \mid i = 1,\ldots,N, j = 1,\ldots,M\}$ so that $u : P \to \mathbb{R}$. We now characterize F-transforms of u for two extreme fuzzy partitions introduced above.*

Largest partition. *The largest partition of $[1,N] \times [1,M]$ contains only one fuzzy set, $A_1 \times B_1$, such that for all $(x,y) \in [1,N] \times [1,M]$, $(A_1 \times B_1)(x,y) = 1$. The respective F-transform component $F[u]_{11}$ and the respective inverse F-transform u_{11} are as follows:*

$$F[u]_{11} = \frac{\sum_{i=1}^{N} \sum_{j=1}^{M} u(i,j)}{NM},$$
$$u_{11}(i,j) = F[u]_{11}, \quad i = 1,\ldots,N, j = 1,\ldots,M.$$

It is easy to see that $F[u]_{11}$ is the arithmetic mean *of u.*

Finest partition. *The finest partition of $[1,N] \times [1,M]$ is established by $N \times M$ fuzzy sets $A_k \times B_l$, such that for all $k = 1,\ldots,N$, and $l = 1,\ldots,M$, $(A_k \times B_l)(x_k,y_l) = 1$, and for all $r = 1,\ldots,N$, and $s = 1,\ldots,M$, such that $(k,l) \neq (r,s)$, $(A_k \times B_l)(x_r,y_s) = 0$. The respective F-transform*

components $F[u]_{kl}$, $k = 1, \ldots, N$, $l = 1, \ldots, M$, and the respective inverse F-transform u_{NM} are as follows:

$$F[u]_{kl} = u(k, l),$$
$$u_{NM}(i, j) = u(i, j), \quad i = 1, \ldots, N, j = 1, \ldots, M.$$

It is easy to see that $u_{NM} = u$.

The following two statements (for the proof see Perfilieva & Valášek (2005)) justify the image-fusion method proposed below. Both are based on the following assumptions: the interval $[a, b]$ is h-uniformly partitioned by $A_1, \ldots, A_n$, where $n > 2$ and $h = (b - a)/(n - 1)$, f is a continuous function on $[a, b]$, $F[f]_1, \ldots and F[f]_n$ are the F-transform components of f with respect to $A_1, \ldots, A_n$.

S1. For each $k = 1, \ldots, n - 1$, and for each $t \in [x_k, x_{k+1}]$ the following estimations hold:

$$|f(t) - F[f]_k| \leq 2\omega(h, f), \qquad |f(t) - F[f]_{k+1}| \leq 2\omega(h, f)$$

where

$$\omega(h, f) = \max_{|\delta| \leq h} \max_{x \in [a, b-\delta]} |f(x + \delta) - f(x)|$$

is the modulus of continuity of f on $[a, b]$.

S2. The k-th component $F[f]_k$ $(k = 1, \ldots, n)$ minimizes the function

$$\Phi(y) = \int_a^b (f(x) - y)^2 A_k(x) dx.$$

3. Image representation for image fusion: step by step

In the next section, two algorithms for image fusion are presented. Both are based on the F-transform technique, leading to one-level or higher-level decomposition of an image; here we explain the technical details of these decompositions. We assume that the image u is a discrete real function $u = u(x, y)$ defined on the $N \times M$ array of pixels $P = \{(i, j) \mid i = 1, \ldots, N, j = 1, \ldots, M\}$ so that $u : P \to \mathbb{R}$. Moreover, let fuzzy sets $A_k \times B_l$, $k = 1, \ldots, n$, $l = 1, \ldots, m$, where $0 < n \leq N, 0 < m \leq M$ establish a fuzzy partition of $[1, N] \times [1, M]$. We begin with the following representation of u on P:

$$u(x, y) = u_{nm}(x, y) + e(x, y), \text{where } 0 < n \leq N, 0 < m \leq M, \tag{5}$$
$$e(x, y) = u(x, y) - u_{nm}(x, y), \forall (x, y) \in P, \tag{6}$$

where u_{nm} is the inverse F-transform of u and e is the respective residuum. If we replace e in (5) by its inverse F-transform e_{NM} with respect to the finest partition of $[1, N] \times [1, M]$ (see the Example above), the above representation can then be rewritten as follows:

$$u(x, y) = u_{nm}(x, y) + e_{NM}(x, y), \forall (x, y) \in P. \tag{7}$$

We call (7) a *one-level decomposition* of u.

If function u is smooth, then the error function e_{NM} is small, and the one-level decomposition (7) is sufficient for our fusion algorithm. However, images generally contain various types of degradation that disrupt their smoothness. As a result, the error function e_{NM} in (7) is not

negligible, and the one-level decomposition is insufficient for our purpose. In this case, we continue with the decomposition of the error function e in (5). We decompose e into its inverse F-transform $e_{n'm'}$ (with respect to a finer fuzzy partition of $[1, N] \times [1, M]$ with $n' : n < n' \leq N$ and $m' : m < m' \leq M$ basic functions, respectively) and a new error function e'. Thus, we obtain the *second-level decomposition* of u:

$$u(x,y) = u_{nm}(x,y) + e_{n'm'}(x,y) + e'(x,y),$$
$$e'(x,y) = e(x,y) - e_{n'm'}(x,y), \forall (x,y) \in P.$$

In the same manner, we can obtain a *higher-level decomposition*

$$u(x,y) = u_{n_1 m_1}(x,y) + e^{(1)}_{n_2 m_2}(x,y) + \ldots + e^{(k-2)}_{n_{k-1} m_{k-1}}(x,y) + e^{(k-1)}(x,y), \text{ where}$$
$$0 < n_1 \leq n_2 \leq \ldots \leq n_{k-1} \leq N,$$
$$0 < m_1 \leq m_2 \leq \ldots \leq m_{k-1} \leq M,$$
$$e^{(1)}(x,y) = u(x,y) - u_{n_1 m_1}(x,y),$$
$$e^{(i)}(x,y) = e^{(i-1)}(x,y) - e^{(i-1)}_{n_i m_i}(x,y), \text{ for } i = 2, \ldots, k-1 \text{ and } (x,y) \in P,$$

which can be rewritten as follows:

$$u(x,y) = u_{n_1 m_1}(x,y) + e^{(1)}_{n_2 m_2}(x,y) + \ldots + e^{(k-2)}_{n_{k-1} m_{k-1}}(x,y) + e^{(k-1)}_{n_k m_k}(x,y). \quad (8)$$

Below, we work with the two decompositions of u that are given by (7) and (8).

4. Two algorithms for image fusion

We propose two algorithms:

1. The simple F-transform-based fusion algorithm (SA) and

2. The complete F-transform-based fusion algorithm (CA).

These algorithms are based on the one-level decomposition (7) and the higher-level decomposition (8), respectively. Moreover, the first algorithm is a special case of the second. Both algorithms are derived from the one developed in Daňková & Valášek (2006).
The main role in fusion algorithms is played by the so-called *fusion operator* $\kappa : \mathbb{R}^K \to \mathbb{R}$, defined as follows:

$$\kappa(x_1, \ldots, x_K) = x_p, \text{ if } |x_p| = \max(|x_1|, \ldots, |x_K|). \quad (9)$$

Note that other definitions of a fusion operator are possible. The choice of a fusion operator is influenced by a type of image degradation encountered. Below, we show that a rather wide class of degradations can be captured by the κ defined above.

4.1 Simple F-transform-based image fusion

Assume that we are given $K \geq 2$ input images $c_1, \ldots, c_K$ with various types of degradation. Our aim is to recognize undistorted parts in the given images and to fuse them into one image. In this section, we describe the algorithm for image fusion based on the one-level decomposition (7).

Each input image c_i, $i = 1,\ldots,K$, is assumed to be a discrete real function $c_i = c_i(x,y)$ defined on the $N \times M$ array of pixels $P = \{(x,y) \mid x = 1,\ldots,N, y = 1,\ldots,M\}$ so that $c_i : P \to \mathbb{R}$. Moreover, the set $[1,N] \times [1,M]$ is assumed to be partitioned by fuzzy sets $A_k \times B_l$, where $k = 1,\ldots,n$, $l = 1,\ldots,m$ and $0 < n \leq N, 0 < m \leq M$. Denote $I = \{1,2,\ldots,K\}$. The algorithm can be summarized as follows:

(1) Decompose input images $c_1,\ldots,c_K$ into inverse F-transforms and error functions using the one-level decomposition (7).

(2) Apply the fusion operator (9) to the respective F-transform components of c_i, $i \in I$, and obtain the fused F-transform components of a new image.

(3) Apply the fusion operator to the to the respective F-transform components of the error functions e_i, $i \in I$, and obtain the fused F-transform components of a new error function.

(4) Reconstruct the fused image from the inverse F-transforms with the fused components of the new image and the fused components of the new error function.

We now proceed with a detailed description of the simple F-transform-based image-fusion algorithm (SA).

Setting:

    Step 0. Choose $n, m, 0 < n \leq N, 0 < m \leq M$, – the numbers of basic functions in the fuzzy partitions of $[1,N]$ and $[1,M]$, respectively.

Initialization:

    Step 1. Create the fuzzy partitions $A_1^{(1)},\ldots,A_n^{(1)}$ and $B_1^{(1)},\ldots,B_m^{(1)}$ of $[1,N]$ and $[1,M]$, respectively.

    Denote $A_1^{(2)},\ldots,A_N^{(2)}$ and $B_1^{(2)},\ldots,B_M^{(2)}$ the finest partitions of $[1,N]$ and $[1,M]$, respectively.

Transformation:

    Step 2. For all $i \in I$, compute the direct and the inverse F-transforms of each input image c_i and obtain:

$$F[c_i]_{11},\ldots,F[c_i]_{nm} \text{ – the F-transform components of } c_i,$$

$$c_{i_{nm}} \text{ – the inverse F-transform of } c_i.$$

    Step 3. For all $i \in I$, compute the error functions: $e_i = c_i - c_{i_{nm}}$. Identify values $e_i(x,y)$, $(x,y) \in P$, with the F-transform components $F[e_i]_{xy}$ of e_i with respect to the finest partitions of $[1,N]$ and $[1,M]$.

Fusion:

    Step 4(a). Apply the fusion operator κ to the respective components of the direct F-transforms of the input images c_i, $i \in I$:

$$\kappa(F[c_1]_{11},\ldots,F[c_K]_{11}) = \kappa_{11}^{(1)},$$

$$\ldots\ldots\ldots\ldots\ldots\ldots\ldots\ldots\ldots\ldots\ldots$$

$$\kappa(F[c_1]_{nm},\ldots,F[c_K]_{nm}) = \kappa_{nm}^{(1)},$$

and obtain the fused F-transform components of a new image:

$$(\kappa_{11}^{(1)}, \ldots, \kappa_{nm}^{(1)}). \tag{10}$$

Step 4(b). Apply the fusion operator κ to the respective components of the direct F-transforms of the error functions e_i, $i \in I$, with respect to the finest partitions of $[1, N]$ and $[1, M]$:

$$\kappa(F[e_1]_{11}, \ldots, F[e_K]_{11}) = \kappa_{11}^{(2)},$$
$$\ldots\ldots\ldots\ldots\ldots\ldots\ldots\ldots\ldots\ldots\ldots\ldots$$
$$\kappa(F[e_1]_{NM}, \ldots, F[e_1]_{NM}) = \kappa_{NM}^{(2)},$$

and obtain the fused F-transform components of a new error function:

$$(\kappa_{11}^{(2)}, \ldots, \kappa_{NM}^{(2)}). \tag{11}$$

Reconstruction:

Step 5. The fused image c is equal to the sum of the two inverse F-transforms with fused components (10) and fused components (11), i.e.:

$$c(x, y) = \sum_{k=1}^{n} \sum_{l=1}^{m} \kappa_{kl}^{(1)} A_k^{(1)}(x) B_l^{(1)}(y) + \sum_{k=1}^{N} \sum_{l=1}^{M} \kappa_{kl}^{(2)} A_k^{(2)}(x) B_l^{(2)}(y), \ (x, y) \in P.$$

4.2 Complete F-transform-based algorithm

In this section, we describe the second algorithm for image fusion, i.e., based on the higher-level decomposition (8). All the assumptions made above remain valid. Moreover, the summarized description of the complete F-transform-based algorithm coincides with the one given above up to the descriptions of their respective decompositions.

We proceed with a detailed description of the complete F-transform-based image fusion algorithm (CA).

Setting:

Step 0. Choose

$k_{\max}$ – maximal number of iterations,

$step$ – coefficient for an increment of the number of basic functions in each fuzzy partition,

n_{start} – starting number of basic functions in the fuzzy partition of $[1, N]$,

m_{start} – starting number of basic functions in the fuzzy partition $[1, M]$,

where $step \leq \min(N - n_{start}, M - m_{start})$ and $0 < n(m)_{start} \leq N(M)$.
Denote $e_i^{(0)} = c_i$ for $i \in I$.

For $k = 0 \cdot step^k$ **to** $k_{\max}$

    Initialization:

Step 1.1. Compute $n = n_{start} \cdot step^k$, $m = m_{start} \cdot step^k$.

Step 1.2. Create fuzzy partitions $A_1^{(0)}, \ldots, A_n^{(0)}$ and $B_1^{(0)}, \ldots, B_m^{(0)}$ of $[1, N]$ and $[1, M]$, respectively.

Transformation:

Step 2. For all $i \in I$, compute the direct and the inverse F-transforms of each function $e_i^{(k)}$ and obtain:

$$F[e_i^{(k)}]_{11}, \ldots, F[e_i^{(k)}]_{nm} \text{ -- the F-transform components of } e_i^{(k)},$$
$$e_{i_{nm}}^{(k)} \text{ -- the inverse F-transform of } e_i^{(k)}.$$

Step 3. For all $i \in I$, compute error functions: $e_i^{(k+1)} = e_i^{(k)} - e_{i_{nm}}^{(k)}$.

Fusion:

Step 4. Apply fusion operator κ to respective components of the direct F-transforms of functions $e_i^{(k)}$:

$$\kappa(F[e_1^{(k)}]_{11}, \ldots, F[e_K^{(k)}]_{11}) = \kappa_{11}^{(k)},$$
$$\ldots\ldots\ldots\ldots\ldots\ldots\ldots\ldots\ldots\ldots$$
$$\kappa(F[e_1^{(k)}]_{nm}, \ldots, F[e_K^{(k)}]_{nm}) = \kappa_{nm}^{(k)},$$

and obtain the fused F-transform components as follows:

$$(\kappa_{11}^{(k)}, \ldots, \kappa_{nm}^{(k)}). \tag{12}$$

Step 5. $k = k + 1$.

End For

Last step of fusion:

Step 6. For all $i \in I$, identify values $e_i^{(k_{max}+1)}(x, y)$, $(x, y) \in P$, with the F-transform components $F[e_1^{(k_{max}+1)}]_{xy}$ of $e_i^{(k_{max}+1)}$ with respect to the finest partitions of $[1, N]$ and $[1, M]$. Apply the fusion operator κ to the respective F-transform components of $e_i^{(k_{max}+1)}$:

$$\kappa(F[e_1^{(k_{max}+1)}]_{11}, \ldots, F[e_K^{(k_{max}+1)}]_{11}) = \kappa_{11}^{(k_{max}+1)},$$
$$\ldots\ldots\ldots\ldots\ldots\ldots\ldots\ldots\ldots\ldots\ldots\ldots\ldots\ldots$$
$$\kappa(F[e_1^{(k_{max}+1)}]_{NM}, \ldots, F[e_K^{(k_{max}+1)}]_{NM}) = \kappa_{NM}^{(k_{max}+1)},$$

and obtain the fused F-transform components as follows:

$$(\kappa_{11}^{(k_{max}+1)}, \ldots, \kappa_{NM}^{(k_{max}+1)}). \tag{13}$$

Reconstruction:

Step 7. The fused image c is equal to the sum of two inverse F-transforms with fused components (12) and fused components (13), i.e.:

$$c(x,y) = \sum_{k=1}^{n_{start}} \sum_{l=1}^{m_{start}} \kappa_{kl}^{(0)} A_k^{(0)}(x) B_l^{(0)}(y) + \ldots$$

$$\ldots + \sum_{k=1}^{N} \sum_{l=1}^{M} \kappa_{kl}^{(k_{max}+1)} A_k^{(k_{max}+1)}(x) B_l^{(k_{max}+1)}(y) \, (x,y) \in P, \quad (14)$$

where $n_0 = n_{start}$ and $m_0 = m_{start}, \ldots, n_{k_{max}+1} = N, m_{k_{max}+1} = M$.

4.3 Justification of the algorithms

By **S1**, a smaller modulus of continuity leads to a higher-quality approximation of an input image by its inverse fuzzy transform. If a certain part of the input image is affected by degradation, then by **S2**, the respective F-transform component captures the weighted arithmetic mean and the error function is close to zero at that part. Thus, by the proposed fusion operator κ, we choose components with maximal absolute values that correspond to those parts of the input image which are least degraded.

5. Experimental results

We tested the algorithms described above on examples of input images which are available at "http://irafm.osu.cz/". Two types of degradations were applied to these images so that they appear as either:

1. multi-focus input images, or

2. multi-sensor input images.

Multi-focus input images are affected by degradation in the form of blurring caused by imaging devices (due to their optical properties or display limitations) and/or the complexity of the image subject. Such images are blurred and noisy and generally exhibit further phenomena such as various motions in the field or input images having different resolutions; these effects were neglected in the subsequent experiments, as our aim was only to minimize blurring and noise in the fused image.

In contrast, multi-sensor input images do not contain a priori degraded information. They can be characterized as more likely to be carriers of complementary information coming from different types of sensors. Of course, additional blurring may occur as well as noise and other distortions in the input images. Here, a fused image should contain the most useful information available in the input images.

The following experiments produced a series of fused images. They differed in their initial settings of the values of the algorithms and thus in their resulting quality. Because the latter is not obvious, we focus on a performance of a particular algorithm and demonstrate various fusions that are better than the input originals. Whenever possible, we compare fused images with ideal images. In this case, the Euclidean distance $E(c,d) = \sqrt{\sum_{x \in P} (c(x) - d(x))^2}$ was used as a measure of quality.

5.1 Multi-focus images

In this section, we demonstrate a multi-focus image fusion. In the first two examples, a Gaussian noise was artificially added to an ideal image at complementary or disjoint regions. In the following two examples, real images made by a digital camera were fused.

Ideally, the fused image is produced by combining regions that are in focus. If this is the case, our fusion operator κ defined by (9) works reasonably well. We can explain (and justify) this as follows: if the one-level decomposition is applied, then the error function of a blurred part is smaller than that of the unblurred (sharp) part. Therefore, the maximal absolute values of the F-transform components reflect the level of sharpness, which is important for fusion. In the case of the SA and CA, an important role is played by the initial settings of the values of the algorithm parameters: the number of basic functions, m, n, in the case of SA and CA and the values of the increment, $step$, and the number of iterations, $k_{\max}$, in the case of CA.

5.1.1 Artificial input images

Figs. 2(d) – 2(f) illustrate the use of the SA and the CA in the case of artificially blurred input images Fig. 2(a) and 2(b). The results show that the best choice was the SA with $m, n = 3$. In this case, the fused image was identical to the original one shown in Fig. 2(c), and for this reason, it is not demonstrated. A lower or a higher number of basic functions propagated the blur into the fused images (see Fig. 2(d), 2(e), and 2(f)), with the respective pictures of the pointwise absolute differences shown in Fig. 2(g), 2(h), and 2(i), where the values that are "close to zero" are in "close to black" color. Moreover, the SA, with the optimal choice $m, n = 3$, has a small computational complexity and was thus very fast. Surprisingly, the CA, with $step = 2$ and 8 iterations (see Fig. 2(f)), did not provide a better fusion.

The next example is slightly different: there are two different Gaussian blurs[1] applied to two disjoint regions of the ideal image Fig. 3(c). Unlike the previous case, we were not able to obtain a fused image identical to the ideal one. The results of our fusion algorithms were as follows: the SA required a rather fine partition, with $m, n = 250$ basic functions (see Fig. 3(e), the Euclidean distance is $E = 75.58$), and the CA slightly outperformed the SA (see Fig. 3(f), the Euclidean distance is $E = 72.53$). However, the computational complexity of the first algorithm (SA) was significantly smaller than that of the second (CA). We finally remark that the application of the simplest SA, with $m, n = 1$ (see Fig. 3(d)), produced a very good fusion with the Euclidean distance $E = 187.07$. The quality of fusion was especially good in the background part of the image.

5.1.2 Real input images
5.1.2.1 Grayscale digital input images

Fig. 4 presents the fusion of multi-focus images originating from a digital camera. Due to space limitations, we show here only the SA output Fig. 4(c) and note that it is comparable (measures of quality are almost equal) to the CA. Because we did not have a whole, ideal image at our disposal, we compare "ideal" parts of the input images with their respective parts in the fused image. These "ideal" parts are designated by the two color boxes in Fig. 4(d), referred to as the "left box" and the "right box". In Fig. 4(e) and Fig. 4(f), we see graphs of the pointwise absolute differences between the "ideal" and blurred parts, where again, the values that are "close to zero" are in "close to black" color. It is easily seen that the quality of fusion in the background region (left box) is better than that in the foreground region (right box). This was

---

[1]A Gaussian blur is a type of an image filter, which combines Gaussian function and the input image by means of convolution.
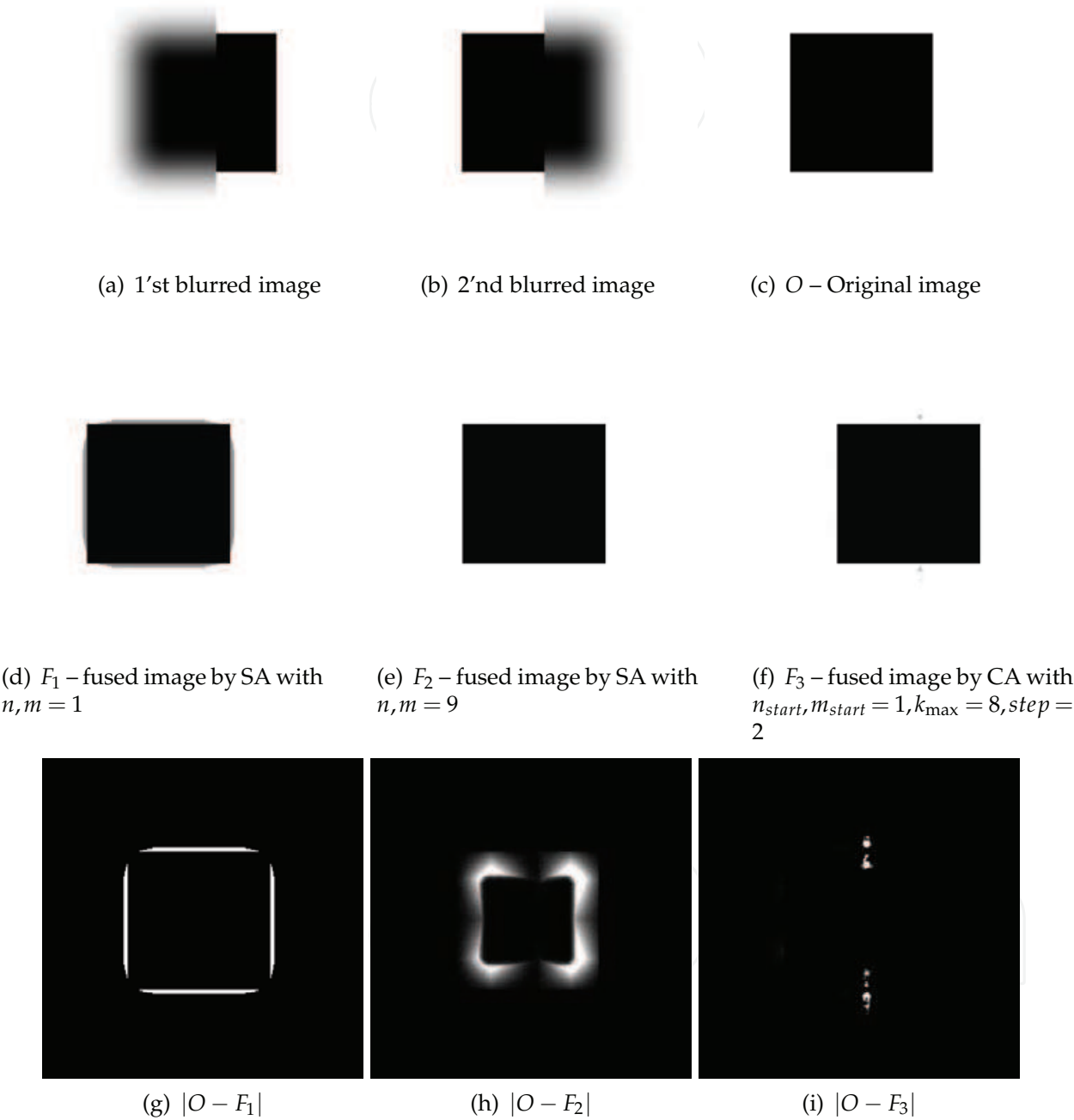
(a) 1'st blurred image

(b) 2'nd blurred image

(c) O – Original image

(d) F_1 – fused image by SA with $n, m = 1$

(e) F_2 – fused image by SA with $n, m = 9$

(f) F_3 – fused image by CA with $n_{start}, m_{start} = 1, k_{\max} = 8, step = 2$

(g) $|O - F_1|$

(h) $|O - F_2|$

(i) $|O - F_3|$

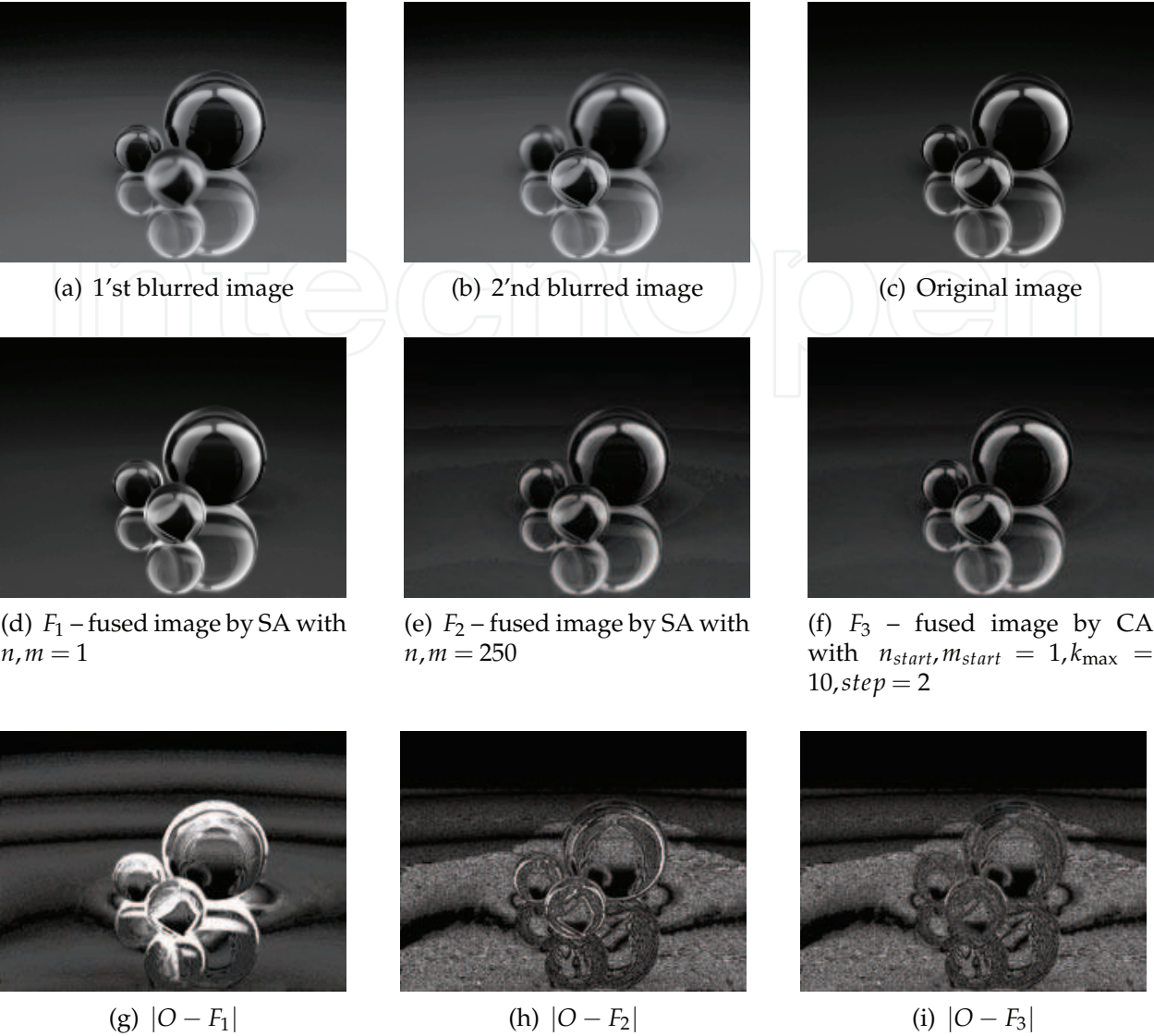Fig. 2. Illustration of various initial setting values of SA and CA applied to a blurred image (Gaussian blur).

(a) 1'st blurred image

(b) 2'nd blurred image

(c) Original image

(d) F_1 – fused image by SA with $n, m = 1$

(e) F_2 – fused image by SA with $n, m = 250$

(f) F_3 – fused image by CA with $n_{start}, m_{start} = 1, k_{max} = 10, step = 2$

(g) $|O - F_1|$

(h) $|O - F_2|$

(i) $|O - F_3|$

Fig. 3. Application of SA to artificially blurred images (Gaussian blur).

caused by differences in reflections from the surfaces of the boxes. It seems that the initial setting values (in our case $n, m = 200$) did not play a significant role in this application.

5.1.2.2 Multichannel color input images

The application shows how the CA can be successfully used for the fusion of multi-focus color images. In our case, the fusion was performed separately for each color component. We assumed the RGB format for input color images and applied the CA with the same initial setting values three times on each R, G and B component. The final fused image was then composed from the fused individual color components.

The input images Fig. 5(a) and Fig. 5(b) depict a rather complicated scene with a lot of different smooth and glossy objects in the background. This observation forced us to choose the CA and not the simpler SA. The resulting (fused) toy in Fig. 5(c) and 5(d) seems to be perfect except for the one blurred area that is still blurred in all the input images. This blurred area is situated in a background area that contains both smooth and glossy elements and is thus

(a) C_1 – 1'st image (right box in focus)

(b) C_2 – 2'nd image (left box in focus)

(c) F – fused image by SA with $n, m = 200$

(d) Regions to compare

(e) $|L - L_{C_2}|$

(f) $|R - R_{C_1}|$
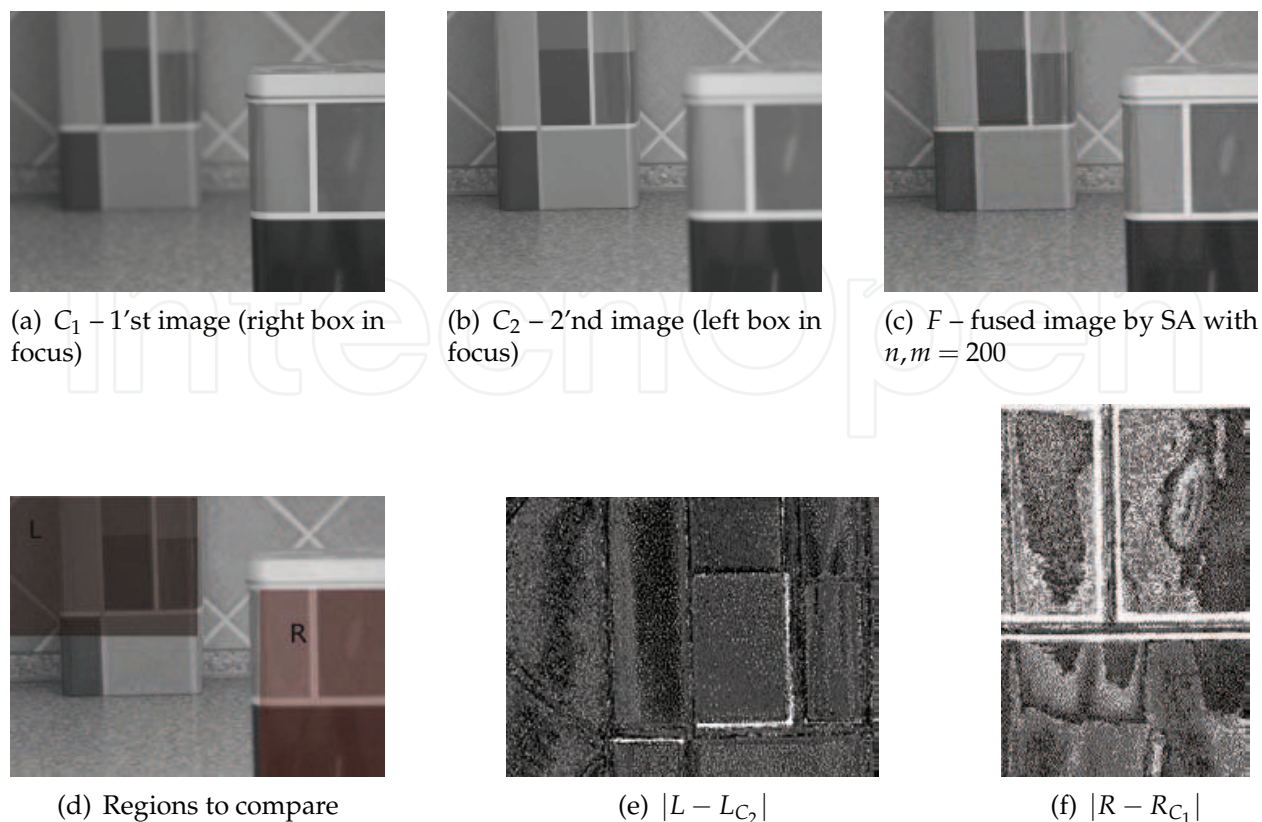
Fig. 4. Application of SA to multi-focus images

very sensitive to any disturbances. Figs. 5(f) and 5(g) present graphs of the pointwise absolute differences (over the region of interest extracted from C_1) between the respective fused images and the first input image in Fig. 5(a). Obviously, the CA with a higher value of n_{start}, m_{start} gives a better fused image (compare Fig. 5(c) and 5(d)).

5.2 Multi-sensor images
This section presents two particular examples of multi-sensor images and their fusion using the F-transform technique.

5.2.1 Image fusion helps navigation
We start with a known benchmark, which can be downloaded from "http://www.metapix.de". It contains two input images taken by two sensors: a thermal imaging forward-looking infrared (FLIR) sensor, depicted in Fig. 6(a), and a low-light television (LLTV) sensor on Fig. 6(b). The sensors were used together in a helmet-mounted display intended for a helicopter pilot. The sensor input images help the helicopter pilot with orientation under poor-visibility conditions. However, they are not both simultaneously at the pilot's disposal. Therefore, image fusion is required. The goal here was to extract and fuse the most important characteristics of the scene, i.e., the paths and their localization in the landscape. In this case, a fast and efficient fusion method is highly desirable.

SA was deemed the most suitable for this application due to its low computational complexity. The results of the SA fusion (see Fig. 6(d)) were compared with the benchmark fusion (available on the same site) based on a multiresolution analysis (see Fig. 6(c)). The quality of our result, shown in Fig. 6(d), is visibly better. The main visual advantage lies in the part
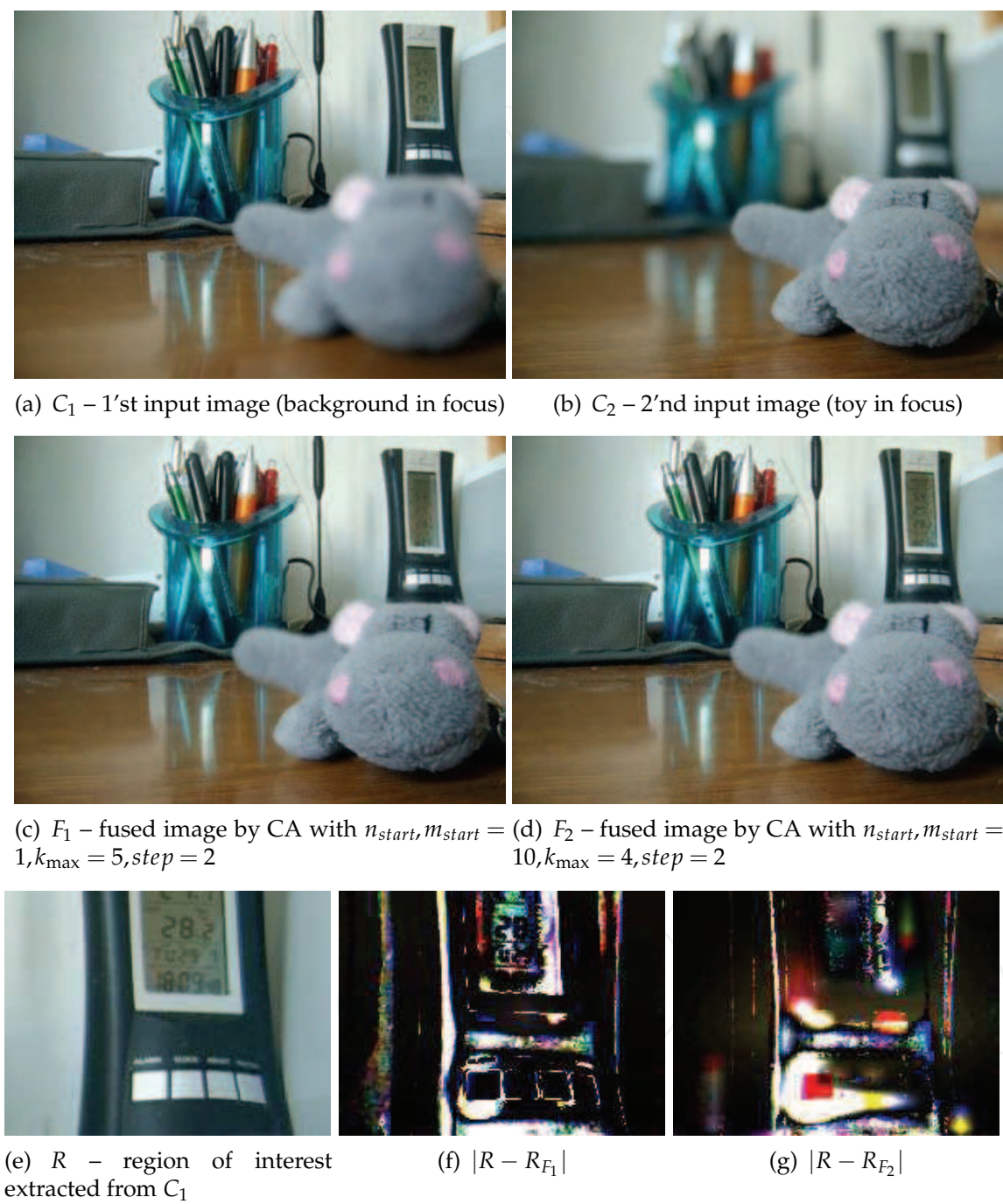
(a) C_1 – 1'st input image (background in focus)

(b) C_2 – 2'nd input image (toy in focus)

(c) F_1 – fused image by CA with $n_{start}, m_{start} = 1, k_{max} = 5, step = 2$

(d) F_2 – fused image by CA with $n_{start}, m_{start} = 10, k_{max} = 4, step = 2$

(e) R – region of interest extracted from C_1

(f) $|R - R_{F_1}|$

(g) $|R - R_{F_2}|$

Fig. 5. Application of CA to multi-focus color images

R marked by the red color in Fig. 6(e); it displays a field. In contrast to the output of the multiresolution analysis, the SA did not change this area. We note that the CA produced a fusion of even better quality (e.g. Fig. 6(f)), although at the cost of higher computational complexity.

5.2.2 Image fusion in medical diagnosis

An important field of applications for image-fusion methods is in medical diagnostics. Imaging methods such as computer tomography (CT), magnetic resonance imaging (MRI) or positron-emission tomography (PET) produce a multitude of images displaying particular information destined for further analysis and interpretation. The significant benefits of image fusion in this field are indisputable and widely sought.

For this application, we used brain MRI images, as in Bloch (2008). These images represent a slice of a dual-echo MRI image acquired with various parameters. As stated in Bloch (2008), the pathology (called adrenoleukodystrophy) is indicated by the bright area in Fig. 7(b) and is not visible in Fig. 7(a). There, the normal structure (ventricles) of a healthy brain is well delineated.

Initial experimental results with the original input images showed that the pure algorithms SA and CA could not be successfully applied. The reason is that Fig. 7(b) is almost uniformly smooth, and the F-transform components corresponding to this image are not within the values of the fusion operator. As can be deduced from the properties **S1** and **S2**, the contrast of an input image is very important for our F-transform-based fusion. Therefore, we modified the original input image in Fig. 7(b) by enhancing its contrast and obtained a new input image, depicted in Fig. 7(c). After this modification, the fusion was again applied to the input images in Fig. 7(b) and Fig. 7(c). The result is shown in Fig. 7(d). The pathological parts as well as the structure of the displayed brain are now nicely visible in the fused image.

6. Conclusion

This study focused on the application of the F-transform to the problem of image fusion. After a brief introduction to the theory of F-transform, detailed descriptions of two fusion algorithms were given. These algorithms are based on one-level and higher-level decompositions of input images. We then proposed an appropriate fusion operator and discussed several types of degradations that can be eliminated by its application.

In various examples, we showed that the proposed approach can be successfully applied in cases when input images are available as either:

1. multi-focus input images or
2. multi-sensor input images.

We examined input images that were artificially blurred and those blurred by inherent restrictions of the imaging tools. For the artificially blurred images, we estimated fusion quality by the Euclidean distance with the origin. For the others, we used the known benchmarks. Last, but not least, we discussed the influence of initial settings of the parameter values of the proposed algorithms on the quality of the resulting fusion.

7. Acknowledgement

(a) FLIR image

(b) LLTV image

(c) Fusion by means of multiresolution analysis

(d) SA $n, m = 100$

(e) Problematic part R

(f) CA with $n_{start}, m_{start} = 40, k_{max} = 3, step = 2$
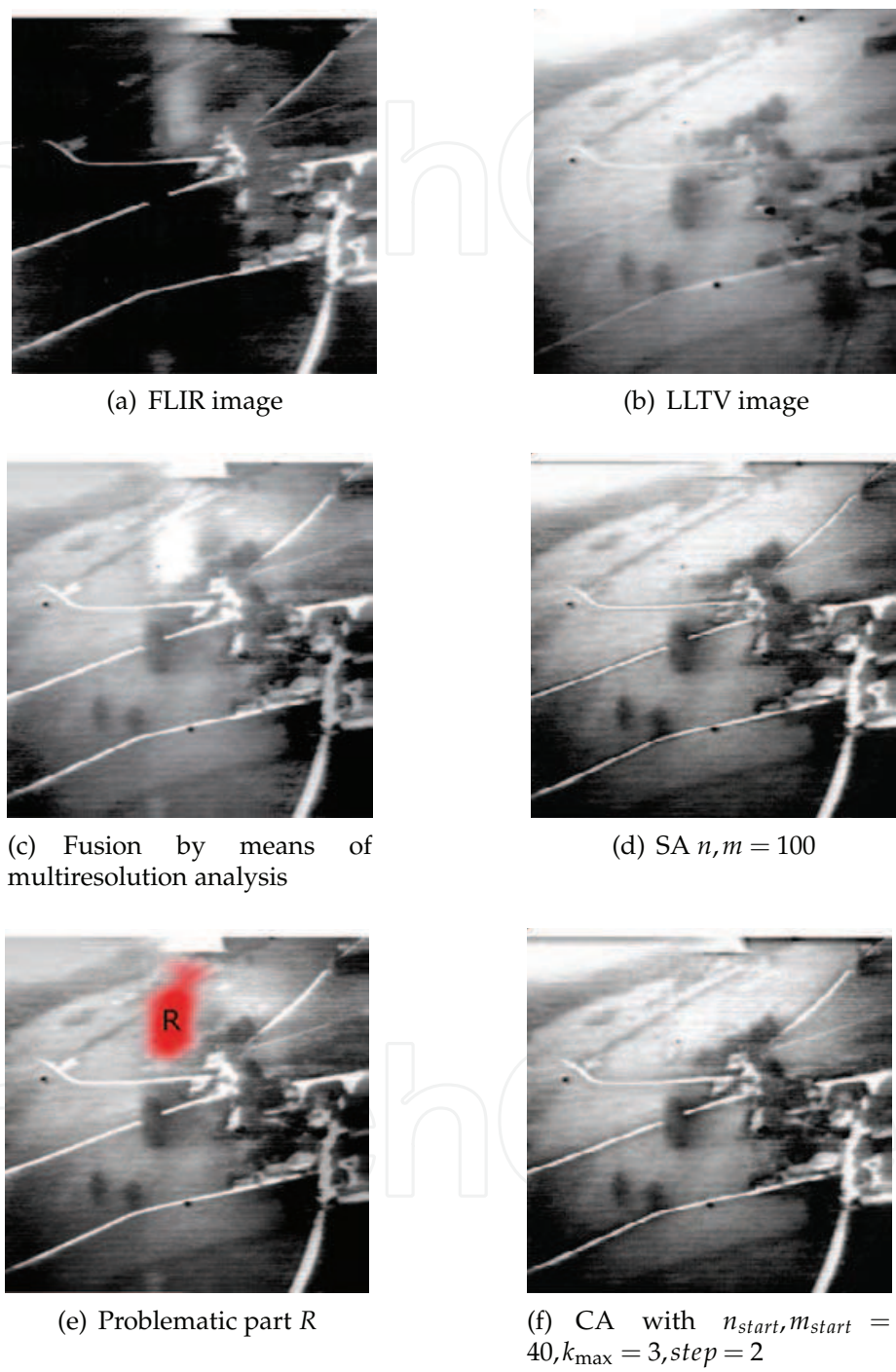
Fig. 6. Illustration of various initial setting values in SA and CA applied to multi-sensor images

(a) 1'st MRI image

(b) 2'nd MRI image

(c) 2'nd image with modified contrast

(d) CA with $n_{start}, m_{start} = 10, k_{max} = 5, step = 2$
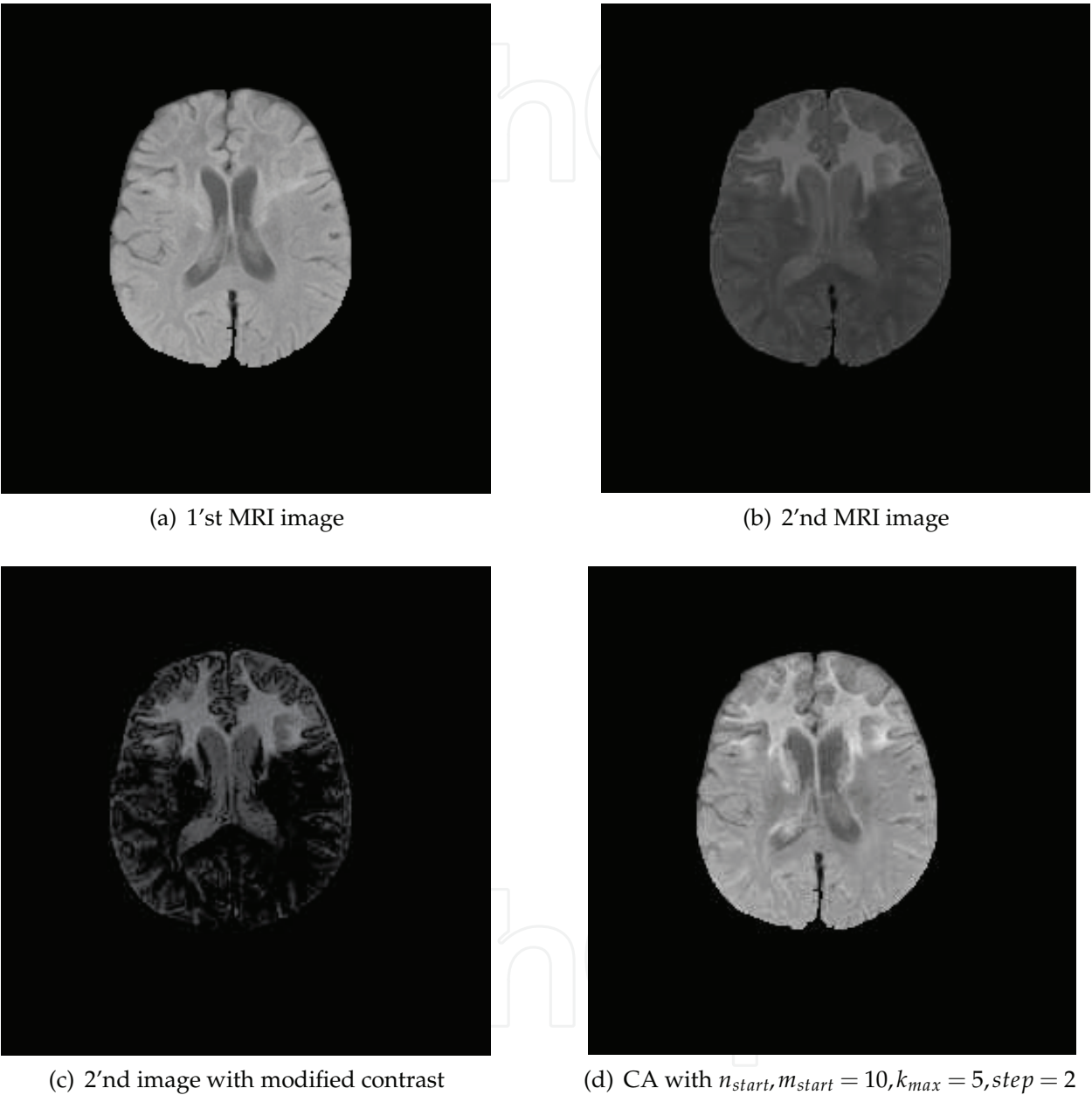
Fig. 7. One axial slice of dual-echo magnetic resonance imaging acquisitions (pathological brain image), courtesy of Professor Catherine Adamsbaum, Saint Vincent de Paul Hospital, Paris.

8. References

Amolins, K., Zhang, Y. & Dare, P. (2007). Wavelet based image fusion techniques – an introduction, review and comparison, *ISPRS Journal of Photogrammetry and Remote Sensing* 62(4): 249 – 263.

Ashoori, A., Moshiri, B. & Setarehdan, S. (2008). Fuzzy image fusion application in detecting coronary layers in ivus pictures, *Communications, Control and Signal Processing, 2008. ISCCSP 2008. 3rd International Symposium on*, pp. 20 –24.

Bloch, I. (2008). Defining belief functions using mathematical morphology - application to image fusion under imprecision, *International Journal of Approximate Reasoning* 48(2): 437 – 465. In Memory of Philippe Smets (1938-2005).

Blum, R. S. (2005). Robust image fusion using a statistical signal processing approach, *Information Fusion* 6(2): 119 – 128.

Constantinos, S., Pattichis, M. & Micheli-Tzanakou, E. (2001). Medical imaging fusion applications: An overview, *Signals, Systems and Computers, 2001. Conference Record of the Thirty-Fifth Asilomar Conference on*, Vol. 2, pp. 1263 –1267 vol.2.

Daňková, M. & Valášek, R. (2006). Full fuzzy transform and the problem of image fusion, *Journal of Electrical Engineering* 12: 82–84.

Loza, A., Bull, D., Canagarajah, N. & Achim, A. (2010). Non-gaussian model-based fusion of noisy images in the wavelet domain, *Computer Vision and Image Understanding* 114(1): 54 – 65.

Mumtaz, A. & Majid, A. (2008). Genetic algorithms and its application to image fusion, *Emerging Technologies, 2008. ICET 2008. 4th International Conference on*, pp. 6 –10.

Perfilieva, I. (2006). Fuzzy transforms: Theory and applications, *Fuzzy Sets and Systems* 157: 993–1023.

Perfilieva, I. (2007). Fuzzy transforms: A challenge to conventional transforms, *in* P. W. Hawkes (ed.), *Advances in Images and Electron Physics*, Vol. 147, Elsevier Academic Press, San Diego, pp. 137–196.

Perfilieva, I. & Daňková, M. (2008). Image fusion on the basis of fuzzy transforms, *Proc. 8th Int. FLINS Conf.*, Madrid, pp. 471–476.

Perfilieva, I., De Meyer, H., De Baets, B. & Plšková, D. (2008). Cauchy problem with fuzzy initial condition and its approximate solution with the help of fuzzy transform, *Proc. of WCCI 2008, IEEE Int. Conf. on Fuzzy Systems*, Hong Kong, pp. 2285–2290.

Perfilieva, I., Novák, V., Pavliska, V., Dvořák, A. & Štěpnička, M. (2008). Analysis and prediction of time series using fuzzy transform, *Proc. of WCCI 2008, IEEE Int. Conf. on Neural Networks*, Hong Kong, pp. 3875–3879.

Perfilieva, I., Pavliska, V., Vajgl, M. & De Baets, B. (2008). Advanced image compression on the basis of fuzzy transforms, *Proc. Conf. IPMU'2008*, Torremolinos (Malaga), Spain, pp. 1167–1174.

Perfilieva, I. & Valášek, R. (2005). Fuzzy transforms in removing noise, *in* B. Reusch (ed.), *Computational Intelligence, Theory and Applications*, Springer, Heidelberg, pp. 225–234.

Piella, G. (2003). A general framework for multiresolution image fusion: from pixels to regions, *Information Fusion* 4(4): 259 – 280.

Ranjan, R., Singh, H., Meitzler, T. & Gerhart, G. (2005). Iterative image fusion technique using fuzzy and neuro fuzzy logic and applications, *Fuzzy Information Processing Society, 2005. NAFIPS 2005. Annual Meeting of the North American*, pp. 706 – 710.

Singh, H., Raj, J., Kaur, G. & Meitzler, T. (2004). Image fusion using fuzzy logic and applications, *Fuzzy Systems, 2004. Proceedings. 2004 IEEE International Conference on*,

Vol. 1, pp. 337 – 340 vol.1.

Šroubek, F. & Flusser, J. (2005). Fusion of blurred images, *in* L. Z. Blum R. (ed.), *Multi-Sensor Image Fusion and Its Applications*, Signal Processing and Communications Series, CRC Press, San Francisco.

Šroubek, Filip, F. J. & Zítová, B. (2006). Image fusion: a powerful tool for object identification, *Imaging for Detection and Identification* pp. 1–20.

Zhang, J. (2010). Multi-source remote sensing data fusion: status and trends, *International Journal of Image and Data Fusion* 1(1): 5 – 24.
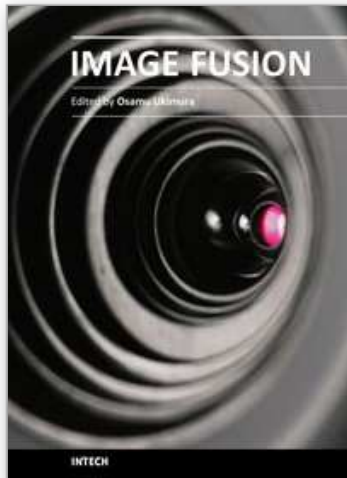
Image Fusion

Edited by Osamu Ukimura

Image fusion technology has successfully contributed to various fields such as medical diagnosis and navigation, surveillance systems, remote sensing, digital cameras, military applications, computer vision, etc. Image fusion aims to generate a fused single image which contains more precise reliable visualization of the objects than any source image of them. This book presents various recent advances in research and development in the field of image fusion. It has been created through the diligence and creativity of some of the most accomplished experts in various fields.

How to reference

In order to correctly reference this scholarly work, feel free to copy and paste the following:

I. Perfilieva, M. Dankova, P. Hodakova and M. Vajgl (2011). F-Transform Based Image Fusion, Image Fusion, Osamu Ukimura (Ed.), ISBN: 978-953-307-679-9, InTech, Available from:
http://www.intechopen.com/books/image-fusion/f-transform-based-image-fusion

INTECH
open science | open minds